V-22 Osprey Aerodynamic Development - A Progress Review

Michael A. McVeigh
John Liu
Stephen J. O'Toole

Boeing Defense & Space Group, Helicopters Division

and

Steven Woods

U.S. Navy

Summary

Events in the aerodynamic development of the multi-service V-22 Osprey tiltrotor are reviewed, with emphasis on recent flight test findings and the solutions developed. A discussion of the performance in the USMC, Navy, and SOCOM missions is presented.

Introduction

The V-22 Osprey (Figure 1) is a multi-service, multi-mission tiltrotor aircraft that incorporates advanced technology to achieve a variety of military tasks. The aircraft combines the hover capabilities of a helicopter with the high-speed, high-altitude performance of a fixed-wing airplane. In 1983, the V-22 design emerged

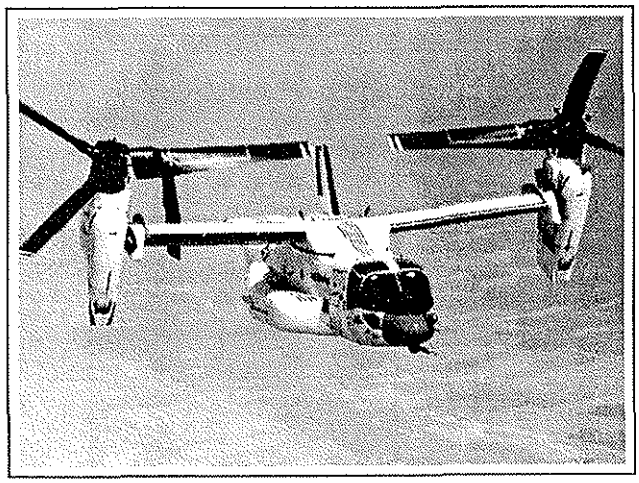

Figure 1. The Bell-Boeing V-22 Osprey

from the concept formulation stage (Figure 2) and entered the preliminary design stage of development. Since then, development has grown through the Full-Scale Development (FSD) phase, which included a flight test program, to the Engineering Manufacturing Development (EMD) phase, wherein four production-representative aircraft are being built and flight tested. Over 1100 flight hours have been accumulated

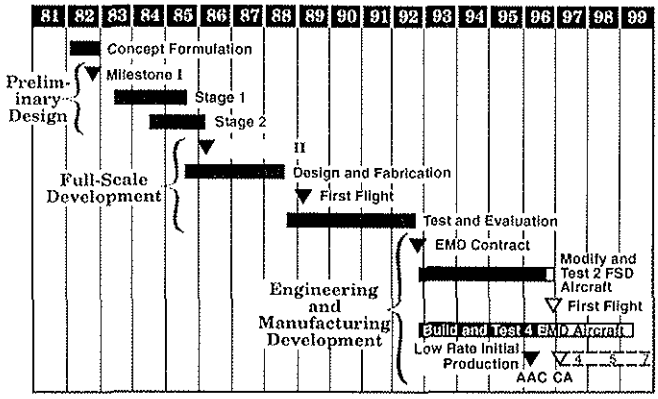

Figure 2. V-22 Program Schedule

on the FSD aircraft. Figure 3 shows the extent of envelope expansion achieved to date. Since the beginning of the program, much has been learned concerning the aerodynamics and performance of tiltrotors.

During the initial design period, the broad dimensions of the aircraft configuration were largely defined by the shipboard-compatibility requirement to fold

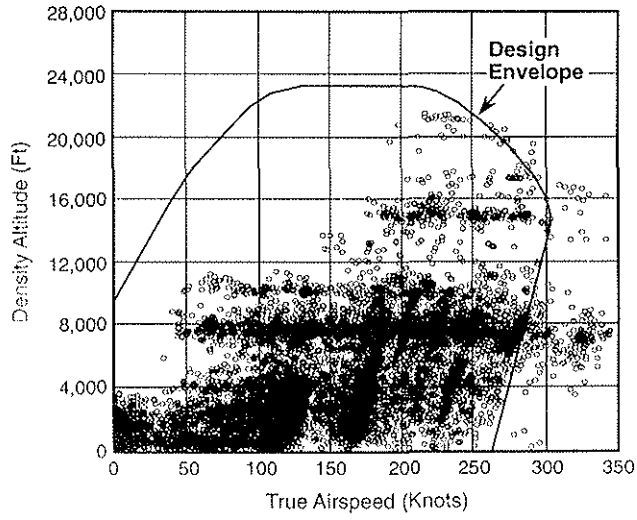

Figure 3. V-22 Design and Flight Test Envelope

and stow on LHA-class ships, and by the requirement to load and carry internally an F-404 engine. These requirements are illustrated in Figure 4, which shows the clearances required and how these defined the rotor diameter, wing span, and rear fuselage upsweep. Thus, no aerodynamic considerations were involved in establishing the most important dimensions of this rotary wing V/STOL aircraft. However, having set these dimensions without reference to aerodynamics, the best efficiency then had to be obtained within these constraints. This was largely achieved by selection of wing and rotor airfoils, blade twist, rotor solidity, and wing chord.

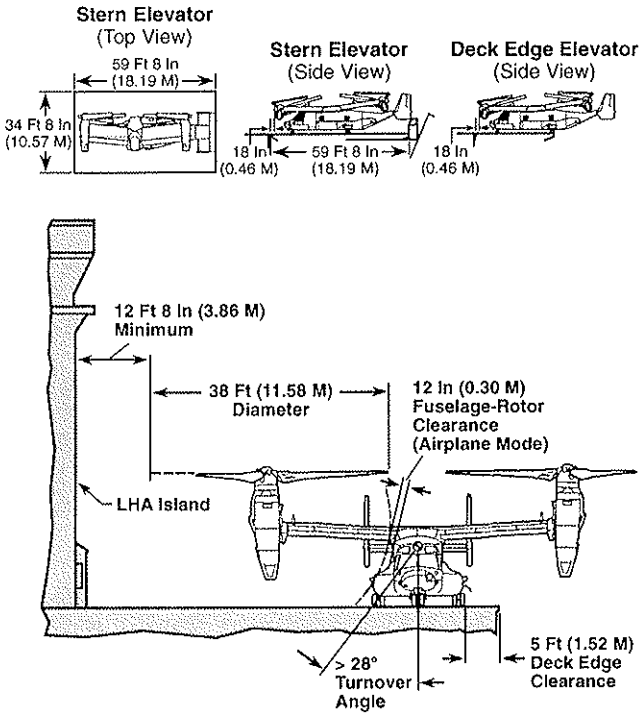

Figure 4. V-22 Osprey Dimensions Are Defined By Shipboard Compatibility Requirements

Airframe configuration definition, performance development, and rotor performance validation progressed in parallel, with the Navy emphasizing validation by testing. This philosophy necessitated an extensive program of wind tunnel testing and tests of a large-scale rotor. This was followed by flight testing of aircraft No. 1 through No. 4 to provide interim data on the FSD configuration, while the modifications to arrive at the EMD configuration were being designed and incorporated in aircraft 7 through 10.

Airframe Development

Wind Tunnel Testing

A series of low-speed wind tunnel tests on the emerging configuration were conducted from 1983 through 1986. Most took place in the 20 feet x 20 feet Boeing Helicopters' large subsonic V/STOL wind tunnel (BVWT). A number of low-speed configuration development tests on powered and unpowered models were conducted, and a high-speed test was made in the Boeing Transonic Wind Tunnel (BTWT). When the FSD configuration was essentially finalized, it was tested up to M=0.72 in the 16-foot transonic tunnel at Arnold Engineering Development Center (AEDC), Tullahoma, Tennessee.

The initial low-speed wind tunnel tests concentrated on the development of wing/fuselage shape, overwing fairing lines, rear fuselage upsweep, and tail configuration. The configuration decisions as to wing sweep, thickness-to-chord ratio, dihedral, and tail configuration are documented in detail in Reference 1.

The results of final tests to determine the full-scale, trimmed, unpowered, low-speed drag polar are shown in Figure 5. The polar was obtained from the unpowered model with vortex generators on the wing leading edge to simulate full-scale Reynolds number effects on C_{Lmax}. The data is corrected for the effects of tunnel buoyancy, tunnel walls, and the drag of the flow-through nacelles. Figure 6 shows the variation of the Oswald induced efficiency factor, e, with lift coefficient. For this wing of aspect ratio 5.5, over the normal operating range of lift, e = 0.82. This value reflects the favorable end-plating effect of the large nacelles.

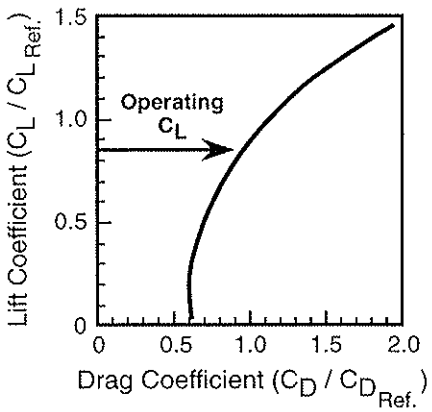

Figure 5. V-22 Trimmed Drag Polar

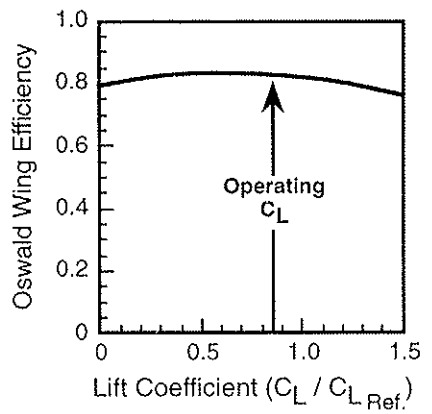

Figure 6. V-22 Airplane Mode Wing Efficiency

As discussed in Reference 2, the presence of the large proprotors produces changes in the airframe drag. Up-inboard rotation of the rotors induces a forward inclination of the local lift vectors whose components

in the free-stream direction act to reduce drag. Based on tests on a powered model, Figure 7 presents the variation of this drag reduction with lift coefficient for two typical values of thrust coefficient.

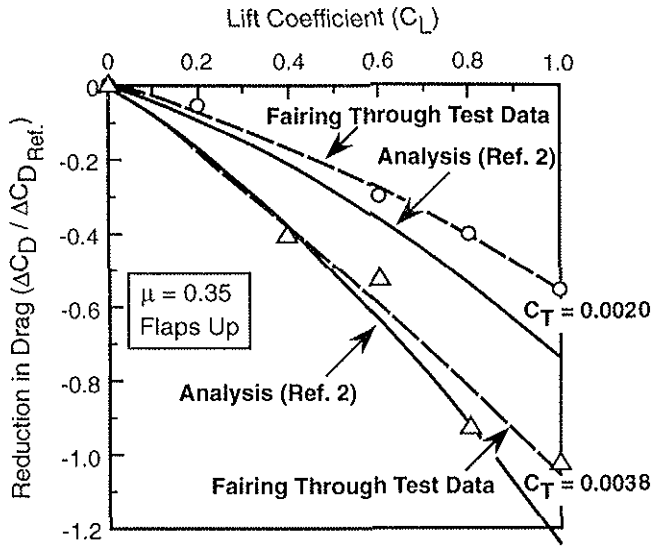

Figure 7. Effects of Up-Inboard Rotor Rotation On Reduction of Aircraft Drag

Flight Test Drag Cleanup and Drag Reduction Program

Early flight tests conducted on FSD aircraft No.1 revealed that the drag was higher, and the maximum lift less, than expected from the wind tunnel results. Detailed inspection of the aircraft showed that there was room for improvement in the quality of surface smoothness, gaps, and steps. The aircraft was therefore subjected to an intensive clean-up program of filling and fairing, the addition of louvers to exhaust exit holes, and the application of vortex generators (VGs) to the wing and overwing fairing. Flight test data (References 3 and 4) showed that the effort was successful and that the lift and drag were more closely in agreement with the wind tunnel results. Figure 8 presents the lift curve showing that the surface smoothness improvement increased C_{Lmax} by 9% and that the addition of VGs raised maximum lift by a further 29%, bringing the results close to the wind tunnel levels. The wing VGs, which were installed at 10% chord, are now part of the configuration. Figure 9 presents the effect on drag, where it is seen that the clean-up lowered the drag by about 6 percent at $C_L/C_{L_{Ref}} = 0.65$ and by 15% at $C_L/C_{L_{Ref}} = 0.85$.

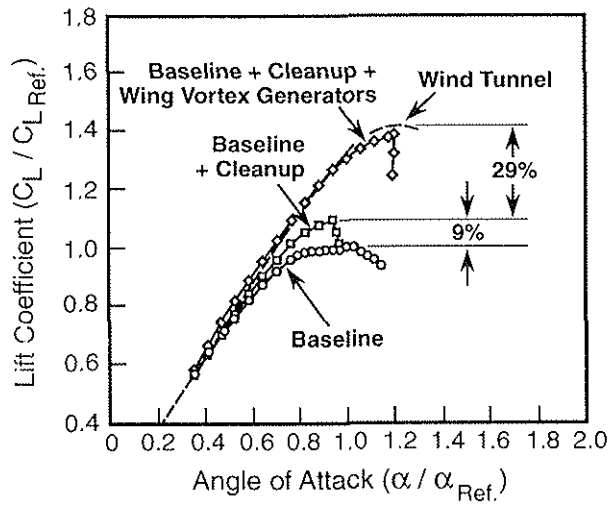

Figure 8. Improvement in Lift Due to Aerodynamic Cleanup

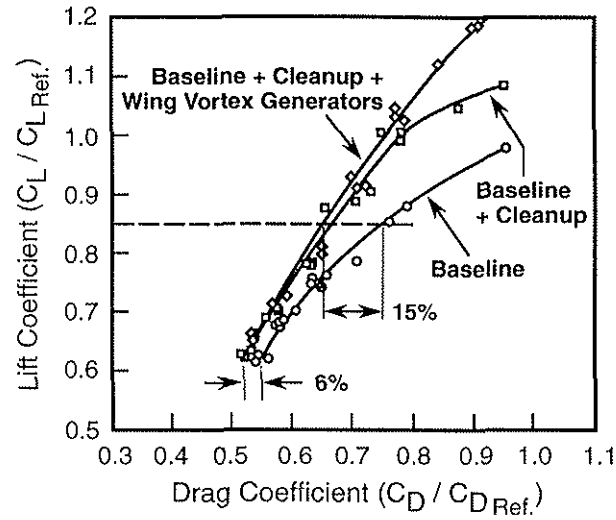

Figure 9. Improvement in Drag Due to Aerodynamic Cleanup

Drag Control Program

In order to ensure that there will be minimal excrescence drag on the EMD aircraft, a drag control program was instituted. An aerodynamic smoothness criteria document was issued defining the guidelines for surface fit-and-finish. All engineering design work that affected the wetted surface of the aircraft was reviewed to ensure compliance with the smoothness guidelines. To further ensure compliance, the aircraft was inspected regularly as they were being built. Inevitably, during manufacture, changes that might increase drag were required and these were evaluated by the aero staff on a case-by-case basis. Figure 10 shows the minimum drag history since the end of FSD,

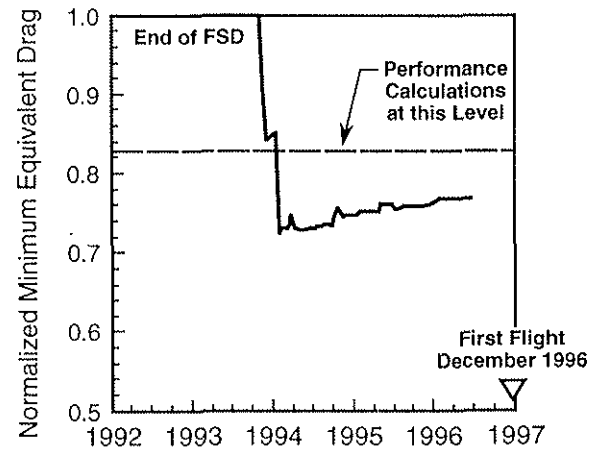

Figure 10. V-22 Drag Reduction Program

when the minimum pre-cleanup drag level of aircraft No. 1 was assessed. Through strict control of excrescence drag, and following a series of design changes including a redesigned engine cooling intake and improved rotor blade cuffs, spinners and hub-mounted pendulum vibration absorbers, it is estimated that the drag of the EMD aircraft will be reduced by about 23 percent The major contributors to the reduction are shown in Figure 11.

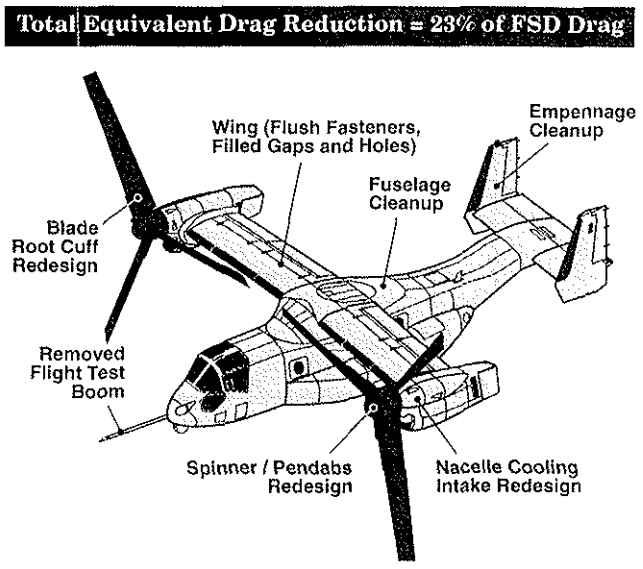

Figure 11. Areas Identified for Drag Reduction

Weight Control

Since the V-22 is a V/STOL aircraft, an aggressive weight reduction program has been in place throughout both FSD and EMD. The weight reduction program relies on realistic weight prediction and a drawing-based, day-to-day assessment of weight growth, combined with vigilant monitoring of the weights of vendor-provided components. As a result of this effort, the empty weight is expected to be about 400 pounds less than the specification empty weight.

Hover Characteristics

Rotor Performance

While the wind tunnel tests of the airframe were proceeding, the rotor development was moving along apace. It was decided that a large-scale test of the rotor was necessary in order to gain confidence in hover performance, since the available analyses at the time were deficient in predicting even the static performance of isolated highly-twisted proprotors, without even considering the effects of a wing beneath the rotors. The test took place at NASA-Ames in March 1984 and the results are reported in References 5 and 6. The main results of these tests were that the download penalty was determined to be 10 percent of thrust, and that the rotor performance was reduced because of rotor downwash being recirculated back into the rotor disc. The data was scaled to the full-scale V-22 and was used in performance predictions.

In the summer of 1994, aircraft No. 2 was flown to Hot Springs, Virginia for a series of tests to establish the aircraft hover performance. This site was selected because it was reasonably close to the base at Patuxent River, Maryland, and, at that time of year, had density altitudes up to 7000 feet for a field elevation of 3792 feet, so that normalized performance would be in the desired range.

In-ground-effect (IGE) and out-of-ground-effect (OGE) flight test data were gathered during free and tethered hover testing. Figure 12 shows the arrangement and Figure 13 presents the results in the form of referred weight vs. referred rotor shaft horsepower. The test data is shown with and without the use of 4 degrees of Opposed Lateral Cyclic pitch (OLC). which is used to tilt the rotor discs

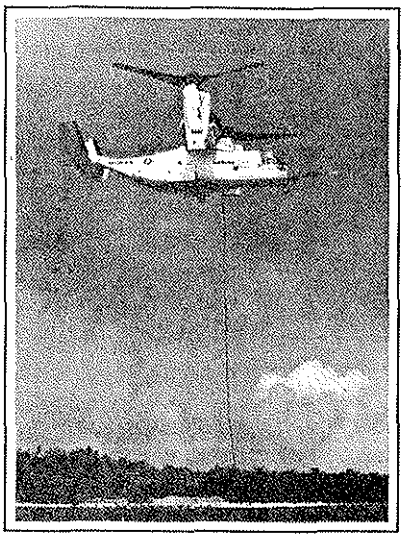

Figure 12. V-22 Tethered Hover Test

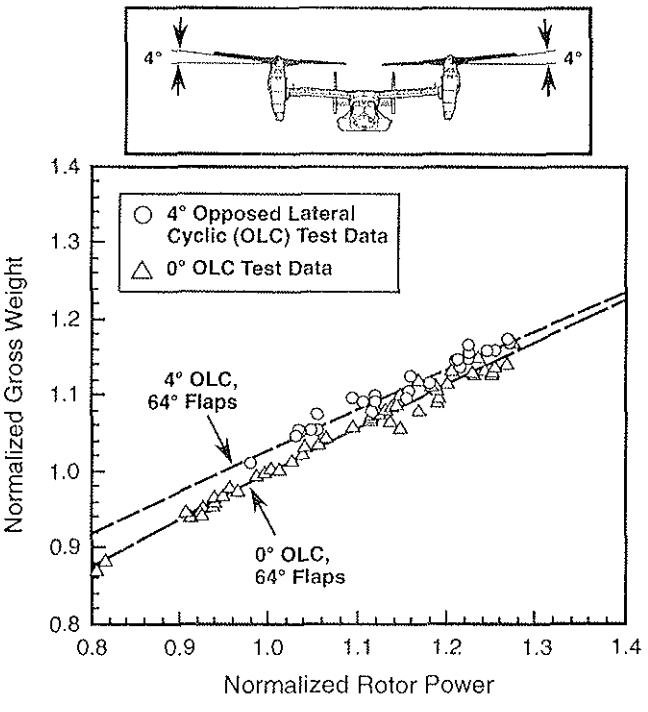

Figure 13. V-22 Out-of-Ground Effect Free and Tethered Hover Performance

laterally down inboard so that the inward movement of the rotor downwash flow impinging on the wing is slowed, which weakens the recirculating flow thereby increasing rotor performance.

OLC is implemented on the EMD aircraft during high performance vertical takeoff. OLC increases hover capability by about 2 percent, on average, at sea level. The measured hover performance is sufficient to accomplish all of the V-22 design missions.

This testing also provided unique visualization of the interaction of the rotor tip vortices with the wing, revealing the asymmetric structure of the vortices and their motion in the recirculating flow. The normal contraction of the wake on the outer portion of the disc, and the reduced contraction of the inner part over the wing were clearly visible, Figure 14a. Though not visible in the figure, the recirculating flow, seen on the Ames tests, was also observed.

The effect of OLC on the wake is also visible in the photos. Figure 14b shows that the wake is deflected outwards, with the trace of the inner wake having moved farther out on the wing.

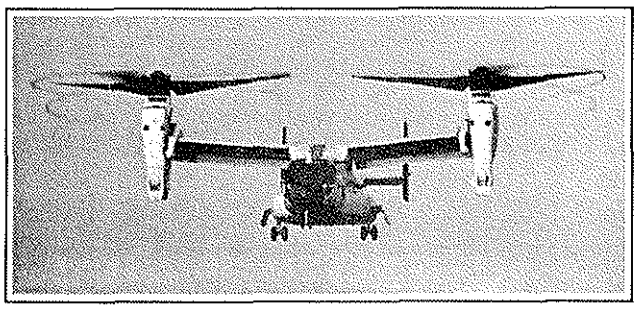

Figure 14 (a). Hover Without Opposed Lateral Cyclic

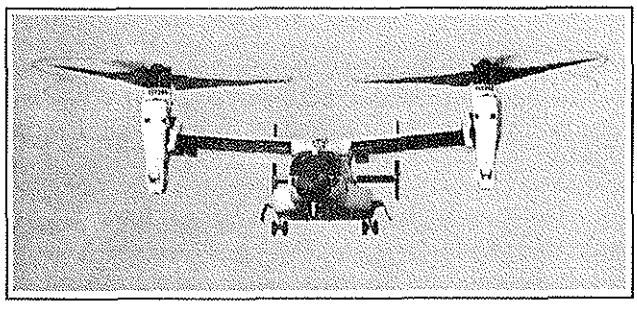

Figure 14 (b). Opposed Lateral Cyclic Deflects Rotor Wake During Hover

Groundwash

As part of operational evaluation testing of the V-22, a series of tests were conducted to determine ground crew workload, and rappeling and fast-roping characteristics. Tests were also conducted to assess the effect of the groundwash from V-22 on neighboring parked aircraft.

The results show that the downwash characteristics do not restrict external load hook-up operations or ingress/egress of ground crew personnel beneath and around the aircraft. With the aircraft hovering at wheel heights from 10 feet to 70 feet, and using loads of 4000 lbs and a HMMWV, no difficulty was encountered in attaching or detaching the load. Limited hovering over water was conducted down to 72 feet to determine the effect on swimmers beneath the aircraft. The minimum hover height was limited to avoid wetting the aircraft external flight test instrumentation. No difficulty was reported by the swimmers.

With the aircraft at 60 feet, rappeling exercises were conducted from the rear ramp. The teams were able to rappel to the targets safely and without difficulty. Fast roping from the cabin door and ramp were also conducted and the team members were able to land close to the targets. No difficulties or problems were encountered when operating a V-22 near other parked aircraft. In summary, data acquired to date indicates that the V-22 groundwash does not present any unusual hazard and that appropriate procedures can be defined for ground support personnel.

Rotor Performance in Cruise

Proprotor propulsive efficiency is based on an axial flow analysis. The analysis was calibrated against limited data acquired in a test of the large-scale isolated rotor in the 40 by 80 feet wind tunnel at NASA-Ames (Reference 7). Figure 15 compares the analysis with the test data. This analysis is used in the flight test data reduction algorithms to deduce lift and drag.

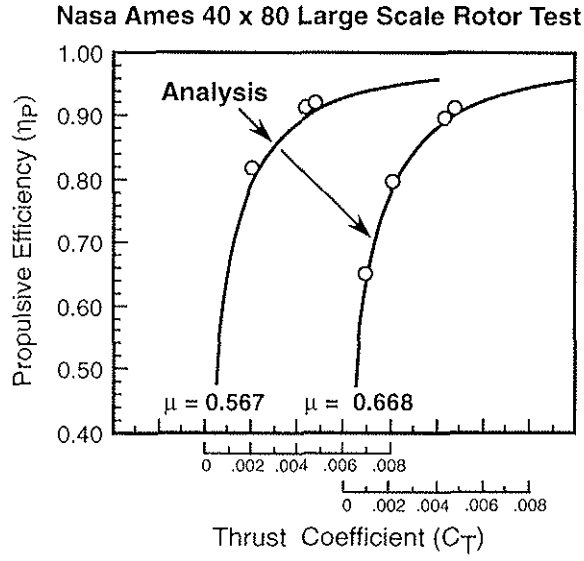

Figure 15. Calculated and Measured V-22 Rotor Cruise Performance

The proprotor develops a significant in-plane normal force which is important to account for in performance calculations. Normal force is calculated, based on results from CAMRAD (Reference 8) correlated with test data on the powered model. Figure 16 presents normal force coefficient as a function of rotor tip-

speed ratio, angle of attack, and thrust coefficient. This data is also used in the flight test algorithms to calculate aircraft performance.

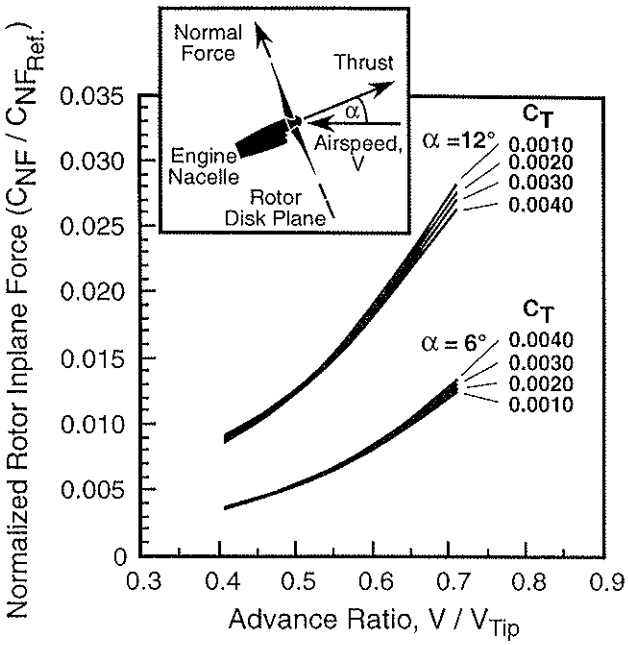

Figure 16. V-22 Rotor In-Plane Force in Airplane Cruise Conditions

Low-Speed Tail Buffet

Early flight testing on FSD aircraft No. 1 and No. 2 showed that the vertical tails were experiencing broadband buffeting during conversion, and that the level of buffeting was maximum when the nacelles were at 60°. Similar buffeting was experienced on the XV-15 and the source of the disturbing flow was identified in full-scale wind tunnel testing as a combination of vortical and separated flow emanating from the nacelle-wing junction. For XV-15, the problem was relieved by reducing the height of the vertical tails to lessen the buffet forces.

The buffet pressures on the V-22 vertical tails excited the second fuselage bending mode resulting in vibration in the cockpit. Clipping the verticals or making structural modifications to the tails were not desired for V-22 because it was estimated that the amount of the reduced span needed would adversely affect lateral stability and any structural changes would add significant cost. An aerodynamic solution was therefore sought.

Tests were conducted in the water tunnel at Wichita State University to investigate ways of altering the disturbing flow at the tail. In airplane mode, with the nacelles horizontal, the wing is end-plated and the tip vortices form outboard of the nacelles. In conversion mode, however, endplating is essentially lost and the wing vortex forms inboard of the nacelle and is thickened and broadened by the flow from the inclined nacelle which acts as a low-aspect ratio wing with its own vortices and separated flow from the rear of the nacelle. The inboard edge of the combined flow moves past the vertical tails and excites them in broadband fashion. The test showed that the phenomenon was difficult to suppress and that the best that could be done was to deflect the flow away from the tails.

The solution developed in the water tunnel was to install wing fences just inboard of the nacelles. Flow visualization showed that fences corral the flow from the wing/nacelle junction and keep it from spreading until the trailing edge is reached. This delay is sufficient to keep most of the flow outboard of the tail, thus reducing vibration. The wing fences are shown in Figure 17. Subsequent flight testing confirmed that the fences reduce the low-speed tail vibration to acceptable levels.

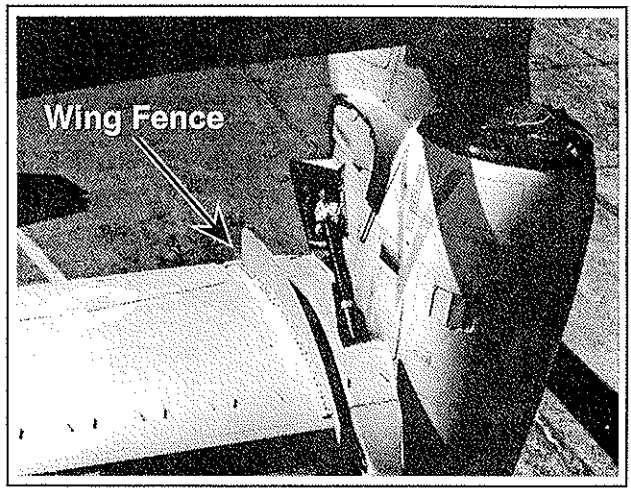

Figure 17. V-22 Wing Fence

High-Speed Tail Buffet

During airplane-mode testing of aircraft No.3 in high-speed, high angle-of-attack, wind-up turns, buffet loads were measured on the horizontal tail that were higher than expected. Unless reduced, these loads would have resulted in unacceptable restrictions being placed on high-speed maneuverability. A program of model tests and CFD analysis was therefore put in place to find the source of the buffeting and to develop an aerodynamic solution that would delay its occurrence to an angle of attack high enough that the desired maneuver envelope could be reached while still maintaining an angle-of-attack margin from buffet.

Wind tunnel and water tunnel tests were conducted on a 1/50th-scale model to obtain a quick qualitative assessment of the source of the buffet. The model was not instrumented and only flow visualization was used to look for causes. Initial impressions were that the sponsons developed strong vortices that passed across the tail at high angles-of-attack, Figure 18. On the basis of these observations, a modification to the

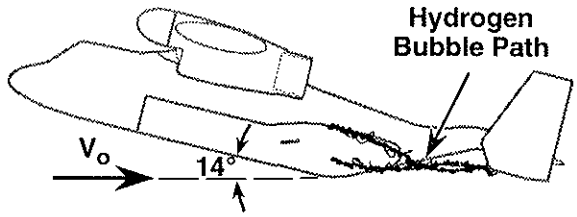

Figure 18. Sponson Vortices Visualized in Water Tunnel Test

model sponson cross-section was developed and tested in the water tunnel. The bottom edges were brought to a small radius and the planform was shaped and swept so as to generate vortices that deflected the disturbing flow from the rear of the sponson away from the horizontal tail. This was called the conical strake, and is illustrated in Figure 19.

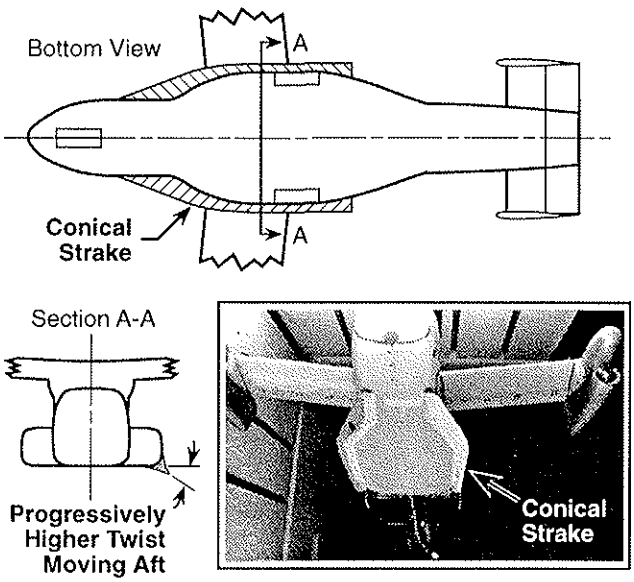

Figure 19. Sponson Conical Strake

The 1/50th-scale tests lacked quantitative data on the problem, so a wind tunnel test of an instrumented 0.15-scale unpowered model was proposed and agreed to by the Navy. The model was tested in the BVWT and was provided with rows of pressure transducers on the empennage and a single row on the overwing fairing to measure the buffet pressures.

The buffet pressures were characterized by root-mean-square (RMS) and power spectral density (PSD) values. Analysis showed that the largest pressures occurred at the top of the fin at 84 percent span and 7 percent chord, and on the horizontal tail at 69 percent span and 7 percent chord.

Figure 20 shows the variation of RMS pressures with angle-of-attack, scaled to full scale, for the horizontal and vertical tails. Figure 21 presents the corresponding variation of lift and pitching moment coefficients. The rapid increases in buffet pressures are seen to

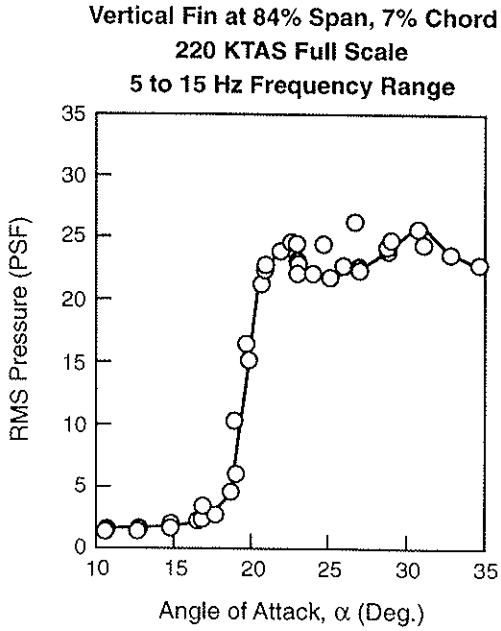

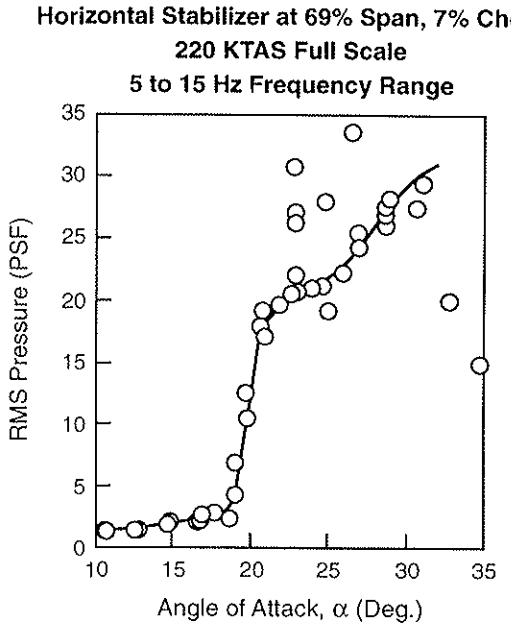

Figure 20. Baseline Variation of Empennage RMS Pressures With Angle of Attack

correspond to the point of initial stall and the pitching moment break, indicating that wing separation might be a contributor. It is also seen that the angle-of-attack for buffet onset on the model agreed with flight test data, thus validating the test.

Runs were then made with the sponsons removed, since these were the suspected prime cause of the buffet. However, no significant change in buffet characteristics was observed. Next the nacelles were removed, with the same result. Finally the wing was removed and the RMS pressures no longer showed the characteristic buffet signature, indicating that separated flow from the wing was indeed the primary cause of buffet.

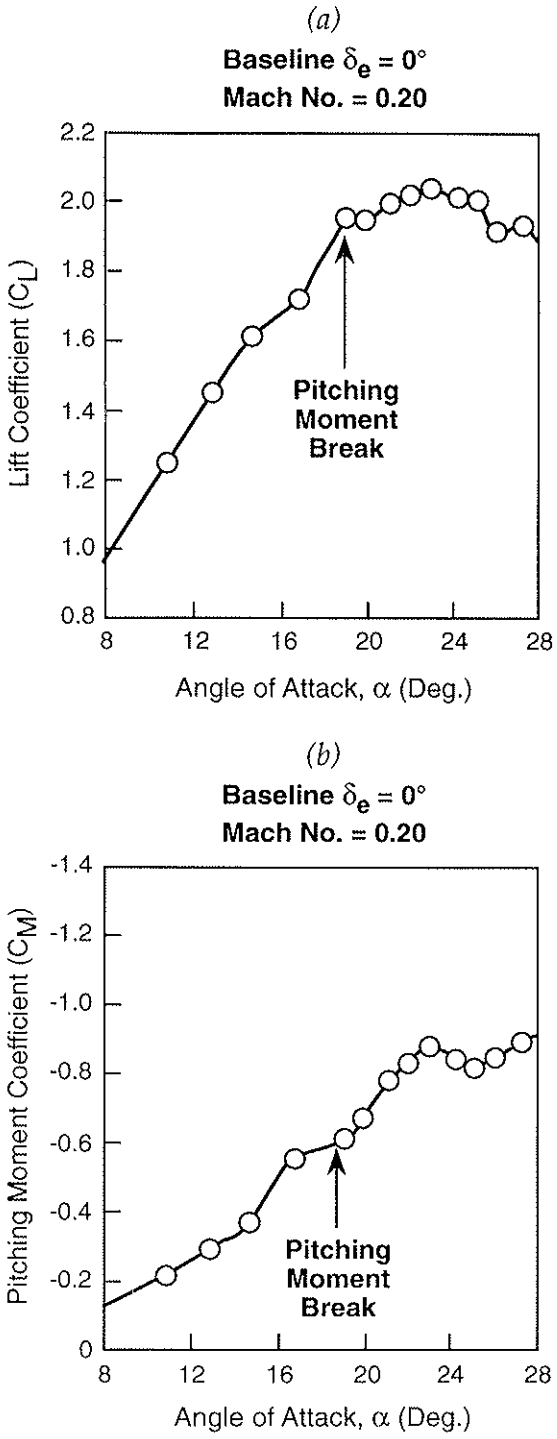

Figure 21. Baseline Aircraft Lift Curve and Pitching Moment

The next step was to find where the separation was located and to delay its occurrence to higher angles-of-attack. The wing surface flow was visualized using oil, and a laser sheet with smoke was used to visualize the flow at the tails. Figure 22 shows the surface oil flow pattern and Figure 23 shows a laser sheet/smoke photo of the flow at the tails. Visualization showed that the wing separated just outboard of the wing/fuselage junction and that this flow was gathered up into a core of separated flow that passed downstream to intersect the vertical tails.

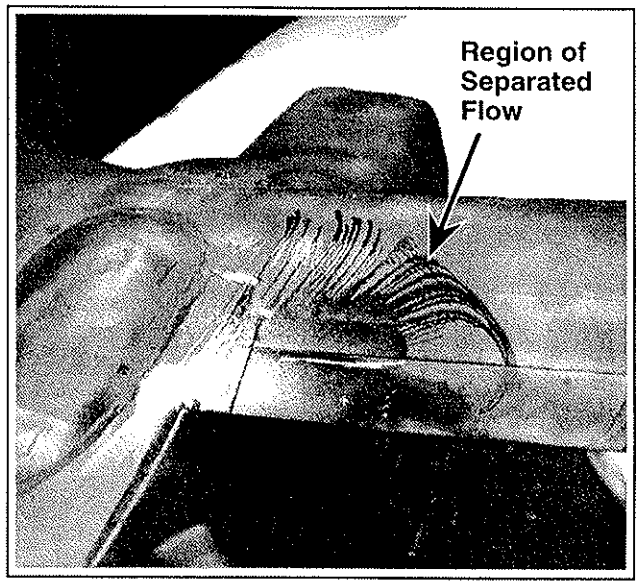

Figure 22. Oil Flow Showing Separated Regions On the Wing

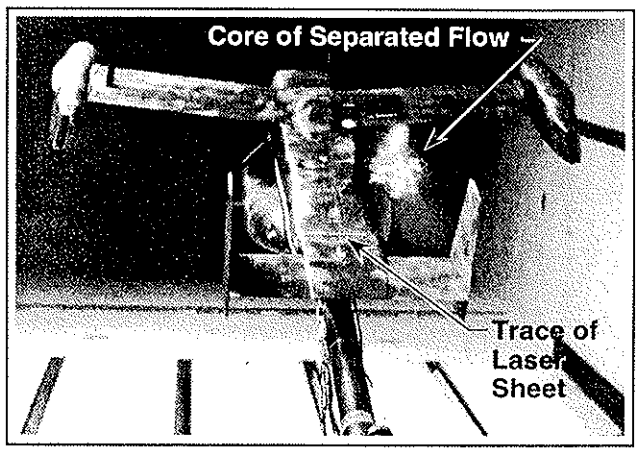

Figure 23. Laser / Smoke System Shows Core of Wing Separated Flow Near Stall

The results of CFD analyses became available to aid in interpreting the results obtained during the tests. The CFD codes were OVERFLOW (analyzed by J. Narramore, Bell Helicopter and E. Meadowcroft, Boeing Helicopters) and CFL3D (analyzed by T.C. Tai, Naval Surface Warfare Center). Both are thin-layer Navier-Stokes methods.

Figure 24 shows the oil flow patterns computed by Meadowcroft at low and high angle-of-attack. At 9° a strong inboard flow at the trailing edge is seen which appears to disturb the flow on the overwing fairing. At 20°, the wing flow is separated at about 50% chord and a large swirling flow has formed over the aft portion of the wing. Figure 25 shows the results of Narramore's computations at an angle-of-attack of 18°. The inward flow at the trailing edge forms two regions of swirling flow on the surface, one just outboard of the wing-fuselage junction, and the other just inboard on the overwing fairing.

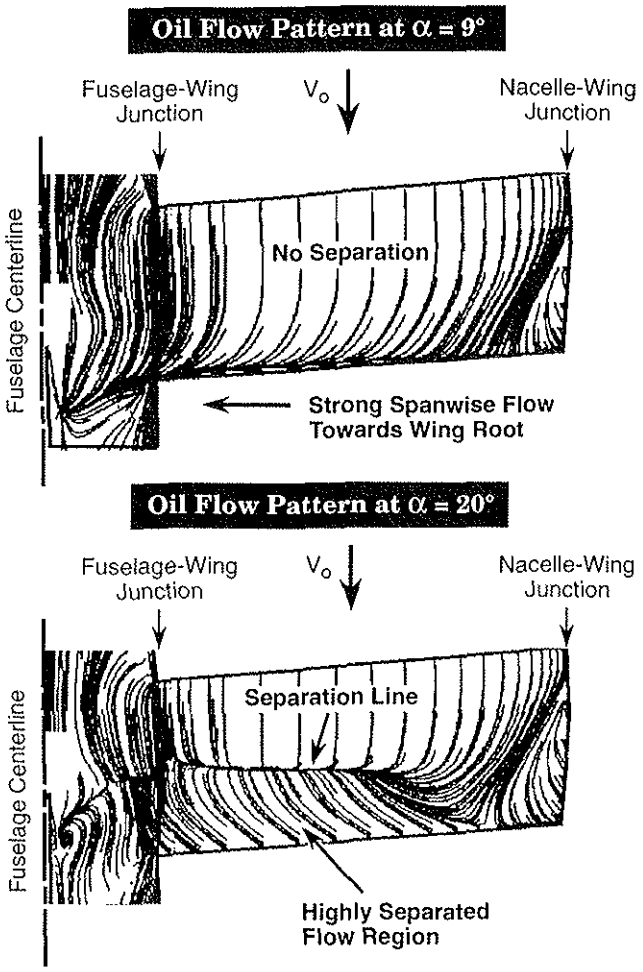

Figure 24. Computed Surface Flow Using OVERFLOW

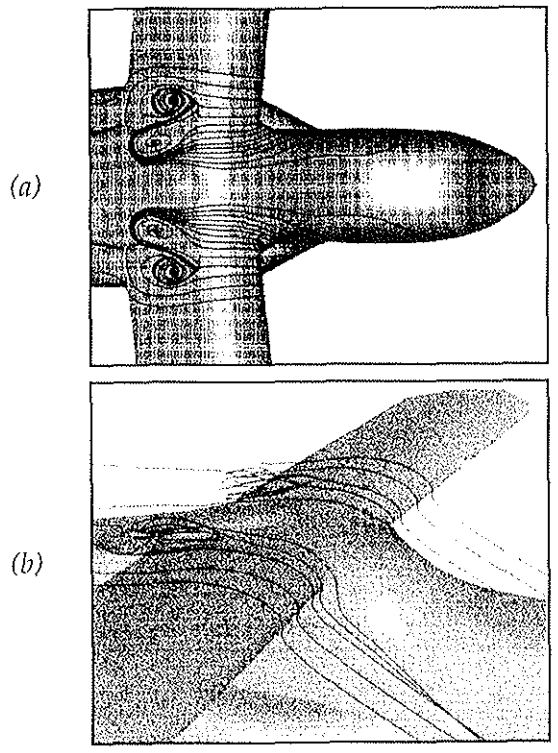

Figure 25. OVERFLOW Analysis Shows Region of Separation at Wing Root and Overwing Fairing, M = 0.4, α = 17.7°

T.C. Tai's results, using CFL3D, shows a very strong inward flow along the trailing edge toward the wing root, the result of the thick separating boundary layer on the 23% thick wing, and the accumulation of this flow into strong streamwise vortices that intersect the vertical tails.

Various methods of delaying the flow separation were tried including leading-edge extensions, wing-mounted vortex generators, wing fences, and the modified sponson shape from the water tunnel investigations (conical strake) Except for the conical strake, nothing was effective. With the conical strake, buffet was delayed by about 4 degrees angle-of-attack. However, the post-stall buffet pressures were significantly increased compared to the baseline. In addition, drag was increased by 1 sq. ft. and static margin was reduced by 25 percent, which was unacceptable.

Tests were then made of vortex-generating strakes placed on the forebody ahead of the wing. The span of a strake at this location on the forebody is limited by considerations of rotor clearance in airplane flight. Various positions, orientations, and sizes of strake were evaluated until the most effective configuration was reached. Figure 26 shows the full-scale embodiment of the most effective strake configuration.

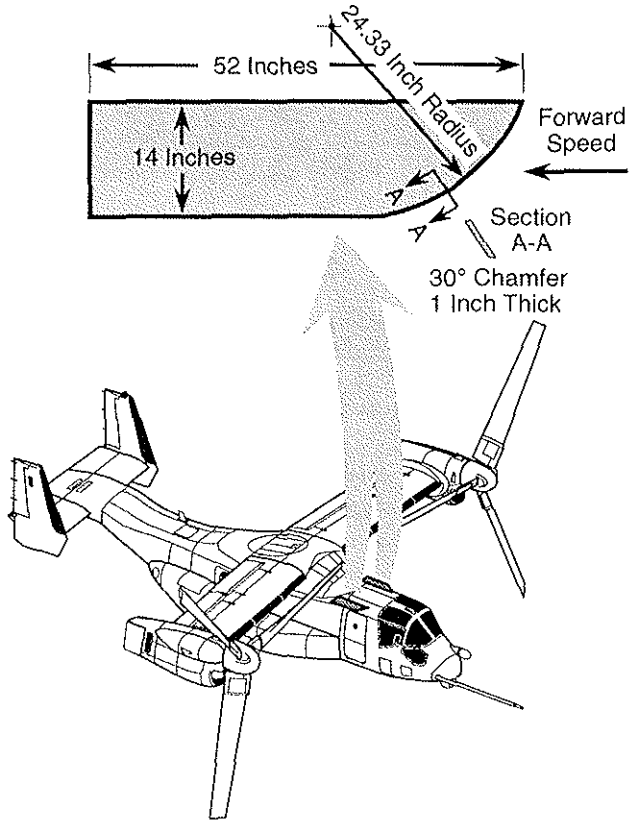

Figure 26. Geometry and Placement of Forebody Strakes

The effect of the forebody strake on buffet pressure is presented in Figure 27. The rapid pressure rise is delayed by 5° and the maximum buffet pressures with the forebody strake in place is less than without the

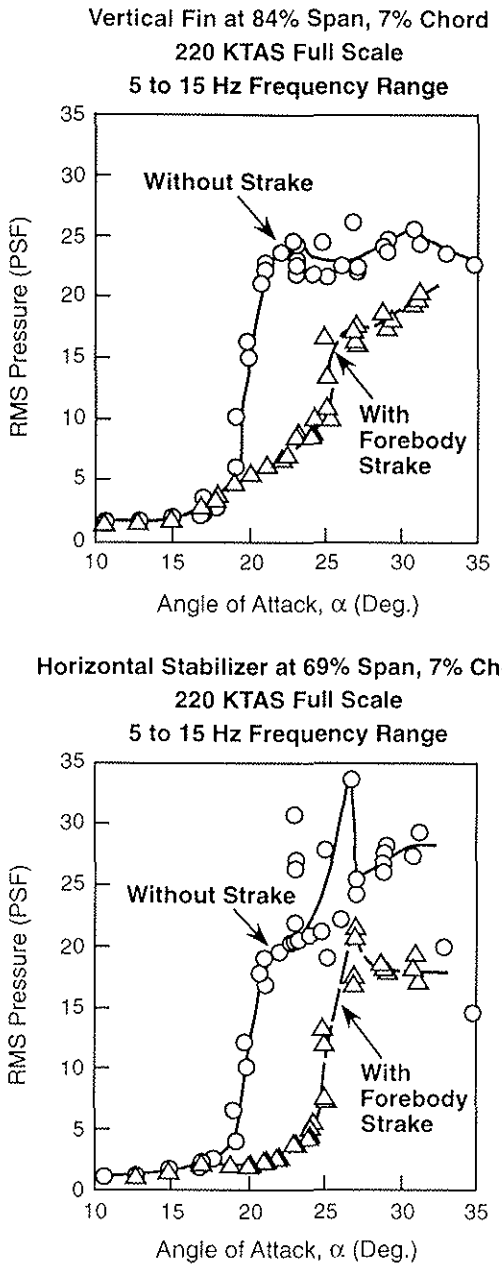

Figure 27. Effect of Forebody Strake On Empennage Buffet Onset

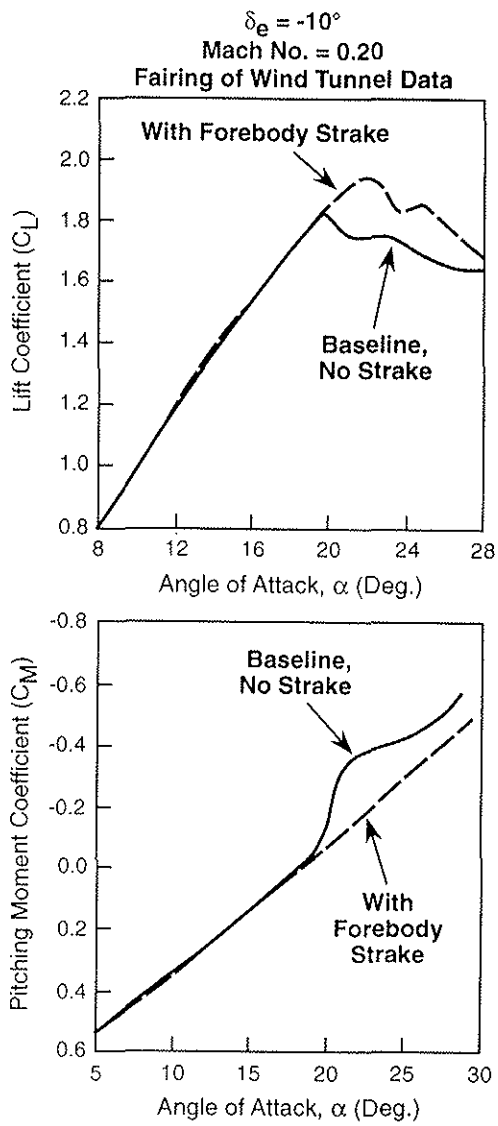

Figure 28. Forebody Strakes Improve Maximum Lift and Linearizes Pitching Moment

strake. Figure 28 shows how the strake increased the lift and linearized the pitching moment. Figure 29 shows how the sideslip boundary is increased by the strake.

A strake was built and flight tested on aircraft No. 3. Figure 30 is a photo of the installation. The results of the buffet testing are presented in Figure 31 which shows that the strake delays buffet onset by about 5°, in agreement with the wind tunnel data. The lift curves of the aircraft, deduced from flight test, with and without the strake are compared in Figure 32 which shows a marked improvement in the stall angle of attack with the strakes. A variation of this strake is now a feature of the EMD aircraft. Further details of the strake development are contained in Reference 9.

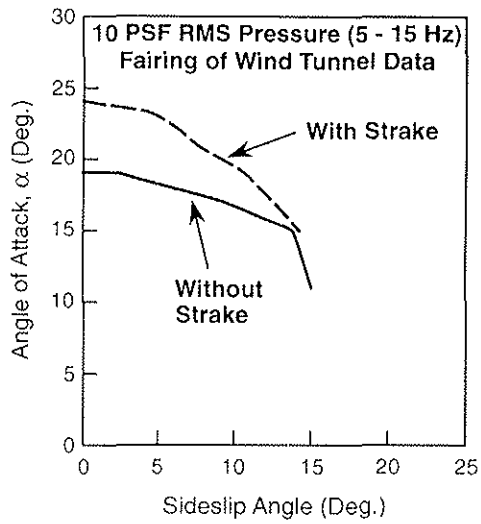

Figure 29. Forebody Strakes Improve Buffet Onset With Sideslip Angle

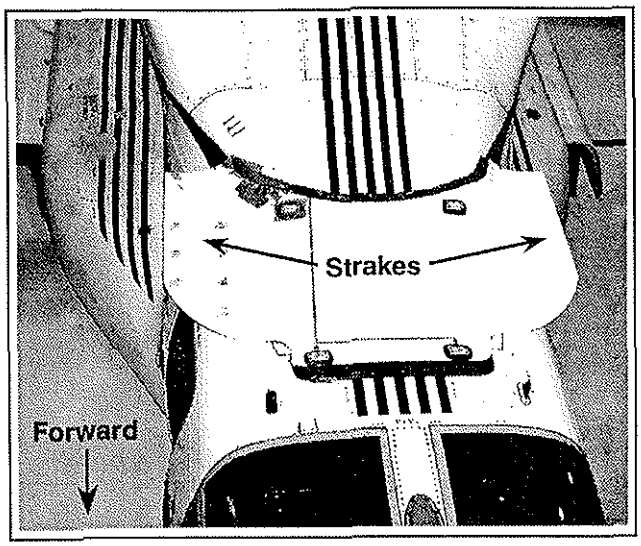

Figure 30. Installation of Forebody Strakes On Aircraft

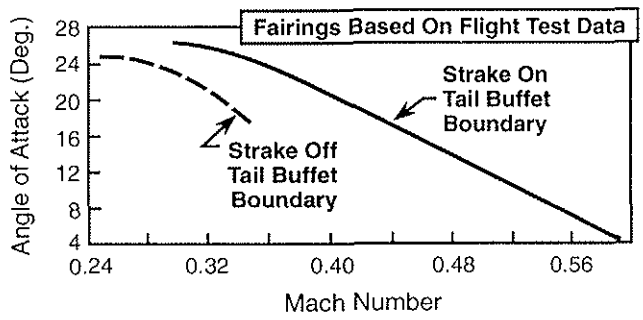

Figure 31. Buffet Onset Angle of Attack From Flight Test Shows Strake Benefit

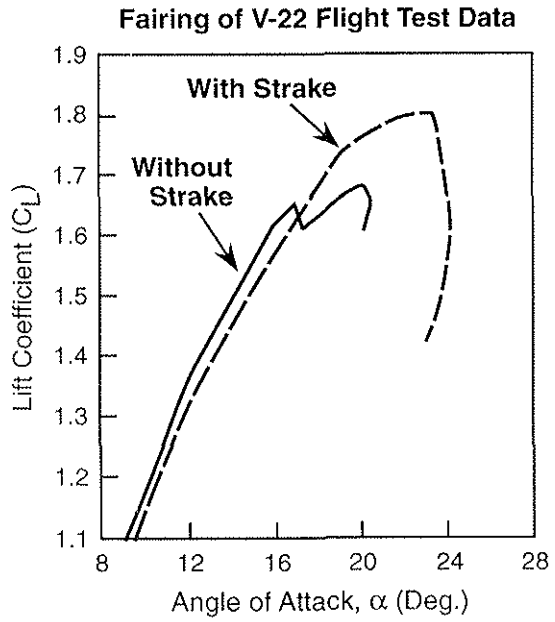

Figure 32. Effect of Forebody Strake On V-22 Lift Curve

Mission Performance

The V-22 is a highly flexible, multi-purpose aircraft capable of performing many missions. Its performance has been evaluated in over thirty different mission scenarios by the US Government, Bell-Boeing, and independent analysis companies.

The design missions for the aircraft are presented in Figure 33. Figure 34 presents the calculated radius capability at the design payloads. As can be seen, the V-22 meets or exceeds the mission requirements.

In each mission, the V-22's high-speed cruise combined with hover capability provides the large area of operations and rapid responsiveness of a fixed wing turboprop aircraft while retaining a helicopter's capability to operate from confined areas. Fewer V-22 aircraft and crews than conventional aircraft and crews are required to cover a given territory or ocean zone.

For the Marine Corps, the Osprey's speed and range provide an expanded battlespace that complicates the enemy's ability to defend. Figure 35 shows the increased combat reach the Marines will have while making an amphibious assault, relative to the capability of the present Marine assault medium lift aircraft, the CH-46. The range capability of the Osprey permits the amphibious fleet to use the sea as operational maneuver space. This increased capability allows greater standoff distance for the amphibious fleet, thus avoiding coastal minefields and missile defenses. It also enhances the element of surprise by providing deception.

Special Operations Forces (SOF) often require high-speed, long-range, V/STOL aircraft capable of penetrating hostile areas. The SOF variant of the V-22, specially outfitted, will meet this requirement. The SOF V-22 is capable of low-visibility, clandestine penetration of medium- to high-threat environments while employing self-defensive avionics and secure, anti-jam, redundant communications. The SOF V-22 can provide long-range self-deployability to maximize mission security and minimize logistics cost. It has an unrefueled combat range sufficient to satisfy current and emergent military needs and carries a built-in refueling boom for range extension. The SOF V-22 possesses the speed to complete most operations within one period of darkness and can operate from air-capable ships without reconfiguration or modification.

With its advanced avionics and vertical takeoff and landing capability, the SOF V-22 can achieve long-distance flights at low-level, at night, and in adverse weather.

Amphibious Assault - Troop Lift (Marine Corps)

- Crew 3
- Payload Of 5760 Lb
- Repeat Mission Unrefueled No Loiter on 2nd Trip
- Fuel Reserve: 20 Min. at V_{BE} or 10% Initial Fuel Whichever is Higher

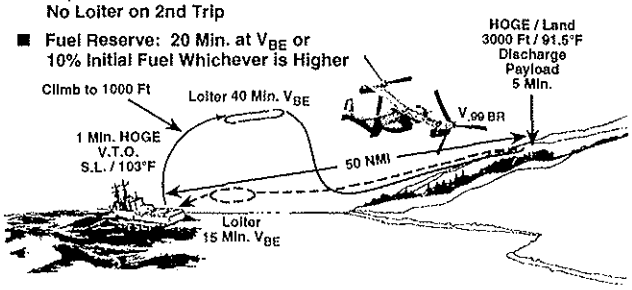

Land Assault - Troop Lift (Marine Corps)

- Crew 3
- Payload 5760 Lb
- Fuel Reserve: 20 Min. at V_{BE} or 10% Initial Fuel Whichever is Higher

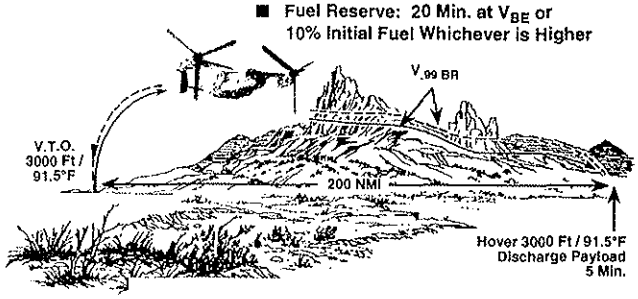

Amphibious Assault - External Cargo Lift (Marine Corps)

- Crew 3
- Payload 10,000 Lb (External)
- Fuel Reserve: 20 Min. at V_{BE} or 10% Initial Fuel Whichever is Higher

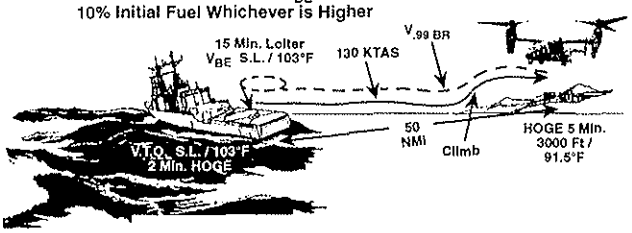

Land Assault - External Cargo Lift (Marine Corps)

- Crew 3
- Payload 10,000 Lb External
- Fuel Reserve: 20 Min. at V_{BE} or 10% Initial Fuel Whichever is Higher

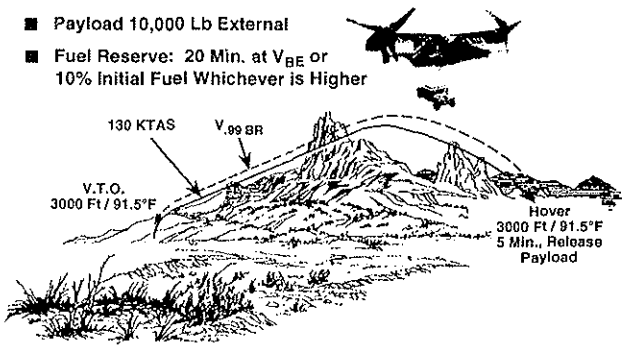

Combat Search and Rescue (Navy)

- Crew 4
- Fuel Reserve: 30 Min. at V_{BE} or 10% Initial Fuel Whichever is Higher

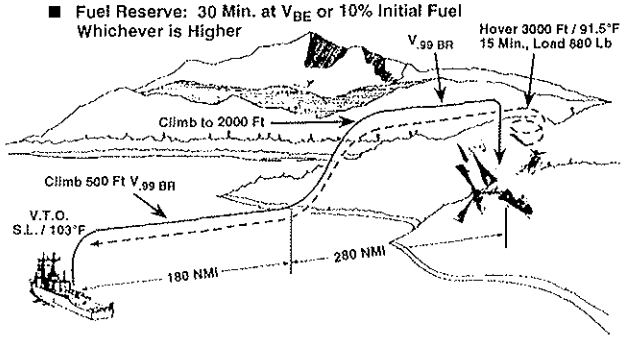

Long Range Special Operations (Air Force)

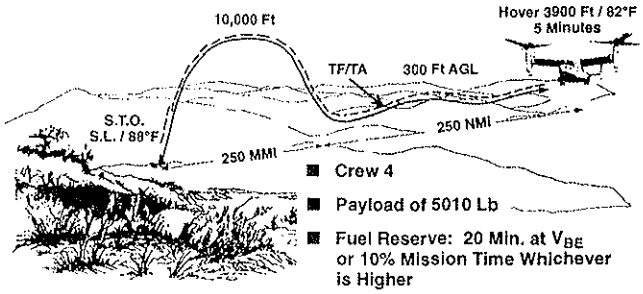

- Crew 4
- Payload of 5010 Lb
- Fuel Reserve: 20 Min. at V_{BE} or 10% Mission Time Whichever is Higher

Pre-Assault / Raid Operations (Marine Corps)

- Crew 3
- Payload of 4980 Lb
- Fuel Reserve: 20 Min. at V_{BE} or 10% Initial Fuel Whichever is Higher

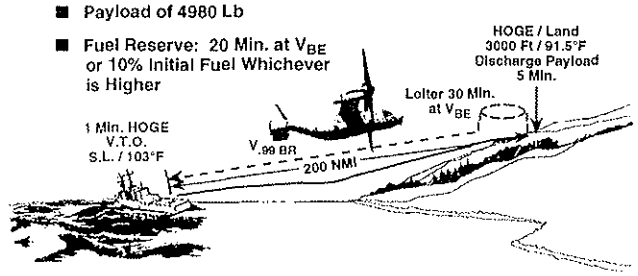

Self-Deployment Intra- / Inter-Theater (All Services)

- Crew 3
- Mission Ready Configuration
- Zero Payload
- Fuel Reserve 10% Initial Fuel
- Prevailing Winds

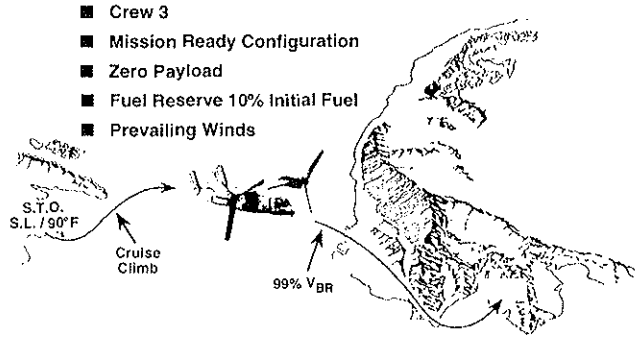

Figure 33. V-22 Design Missions

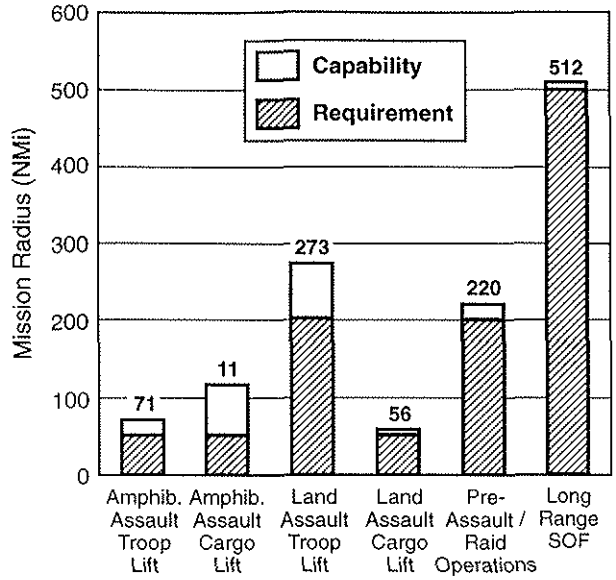

Figure 34. V-22 Mission Radius Capability at the Design Payloads

V-22 Capability

Expands Battlespace / Complicates Enemy's Problem

- **Standoff ... uses maneuvering space of the sea**
- **Surprise / deception**
- **Penetration -- much greater**

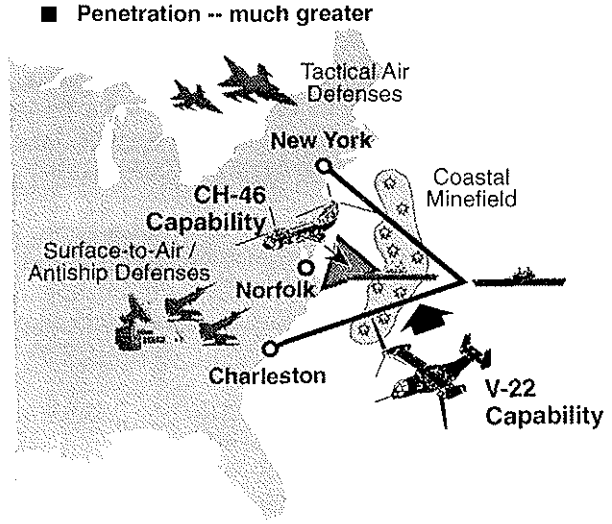

Figure 35. Enhanced Reach in War

The SOF V-22 requirements are:

- Fly at least 500 nmi unrefueled, locate a landing point within 80 ft, and hover out of ground effect (HOGE) at 3900 ft/82°F at the mission mid-point while carrying at least 18 fully-loaded troops.
- Cruise at speeds greater than 230 knots at low level (300 ft AGL), using terrain-following flight sensors and techniques at night and in adverse weather.
- Self-deploy 2100 nmi worldwide with a single air refueling.
- Minimize acoustic, infrared, and visual signatures.
- Carry 10,000 lb internally or externally.
- Refuel air-to-air.

Figure 36 portrays the use of the V-22 in the initial stage of "Operation Eastern Exit", the evacuation of 61 Americans and several foreign Ambassadors from the US Embassy in Mogadishu, Somalia. The actual evacuation by CH-53Es, delivered by the *USS Trenton* (LPD-14) from its anchorage off Oman to the Somali coast, took 87 hours and included three aerial refuelings per helicopter. If the V-22 had been available, the same mission could have been flown directly from Oman using two aerial refuelings with a total mission time less than seven hours.

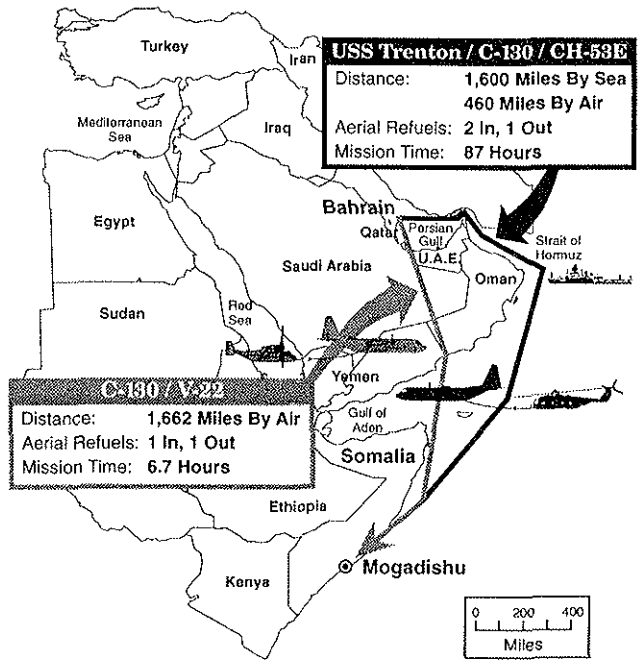

V-22 Speed and Range Reduce Reaction Time

Figure 36. Operation Eastern Exit - Helicopter vs. V-22

Figure 37 shows how the V-22 would have benefited the attempted April, 1980 rescue of US Embassy personnel held hostage in Iran. The use of V-22 would have eliminated the refueling at Desert One where the mission had to be aborted. The V-22 would have also eliminated additional concerns over deploying, mission time, nighttime navigation and shipboard compatibility.

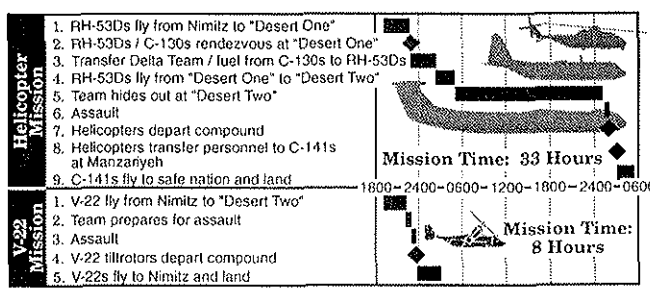

V-22 Speed and Range Increase the Likelihood of Success

Figure 37. Desert One Scenario - Helicopter vs. V-22

The Search and Rescue variant of the V-22 is a long-range aircraft capable of conducting rescue operations requiring a hover over land or water. Typical SAR

missions often require extended range and speed requirements combined with extended time-on-station to perform the necessary search. The ability to combine speed, range, and time-on-station with the ability to hover to recover personnel, means the SAR V-22 can provide a great improvement over the capabilities of current SAR aircraft.

An illustration of the SAR capability of the V-22 is shown in Figure 38. Flying from two or three airfields in Sweden, the V-22 could perform SAR missions covering all of Scandinavia and the East Baltic Republics, along with large areas of Germany, Poland, the Norwegian Sea and the North Sea.

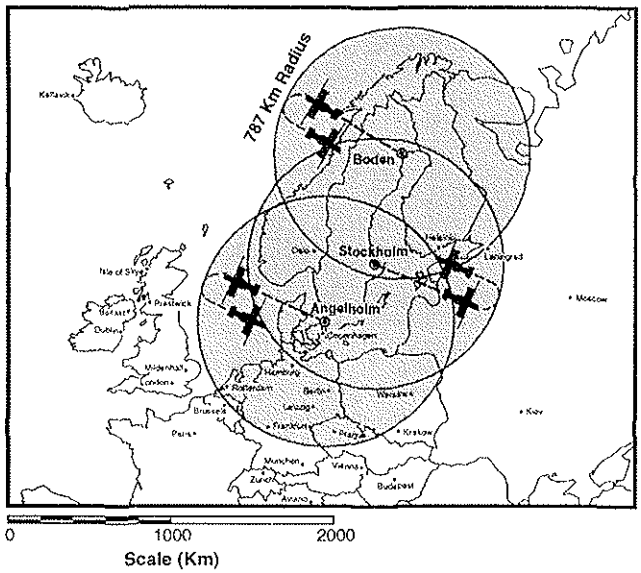

Figure 38. V-22 Search and Rescue

Conclusions

Recent developments in the aerodynamics and performance of the V-22 Osprey have been reviewed. The main points discussed were:

(1) The wind tunnel tests showed the importance of rotor slipstream effects on the drag polar and demonstrated that the endplating effects of the nacelles improve wing induced efficiency.

(2) Because of the thick wing airfoil, vortex generators are required both on the model and on the aircraft to achieve high levels of C_{Lmax}.

(3) A flight test excrescence drag reduction program demonstrated a reduction in the minimum drag level of six percent.

(4) The hover performance of the aircraft has been measured in flight test and is adequate to accomplish all the design missions set for the aircraft.

(5) A tail buffet problem, experienced in flight test, was solved in the wind tunnel and the solution demonstrated in flight.

(6) Large gains in mission capability and operational effectiveness are projected using the V-22.

Acknowledgements

The authors wish to thank all the members of the Bell-Boeing team and the NAVAIR technical community who contributed to the successful developments reported in this paper. Special thanks to Ken Bartie and Nick Dorofee for preparing the paper.

References

1. Rosenstein H., and Clark R., "Aerodynamic Development of the V-22 Tiltrotor", AIAA/AHS/ASEE Aircraft Systems, Design and Technology Meeting, October 20-33, 1986, Dayton, Ohio.

2. McVeigh M. A., Grauer, W.K., Paisley, D.J. ,"Rotor/Airframe Interactions, on Tiltrotor Aircraft", Journal of the American Helicopter Society, Vol.35, (3), July, 1990.

3. Grauer W.K., and Farrell M.K., "V-22 Flight Test Aerodynamics", AHS 47th Annual Forum, Phoenix, Arizona, 1991.

4. Savage M.C., Grauer W.K., Farrell M.K., and McVeigh M.A., "V-22 Flight Test Aerodynamic Refinement", AHS 49th Annual Forum, St. Louis, Missouri, May 19-21, 1993.

5. Felker, Fort F., Maisel, Martin D., and Betzina, Mark D.,"Full Scale Tiltrotor Hover Performance", presented at the 41st Annual Forum of the American Helicopter Society, May 15-17, 1985.

6. McVeigh, M.A., "The V-22 Tiltrotor Large Scale Rotor Performance/Wing Download Test and Comparison with Theory", Eleventh European Rotorcraft Forum, London, England, 1985, Paper No. 97.

7. Felker, F.F., "Results from a Test of a 2/3 Scale V-22 Rotor and Wing in the 40-by-80 Wind Tunnel", presented at the 47th Annual Forum of the American Helicopter Society, Phoenix, Arizona, March 1991.

8. Johnson W., "A Comprehensive Analytical Model of Rotorcraft Aerodynamics and Dynamics - CAMRAD", Volumes I & II, User's Manual.

9. McVeigh M.A., Liu J., and Wood, T., "Aerodynamic Development of a Forebody Strake for the V-22 Osprey", AHS 51st Annual Forum, May 9-11, 1995.

10. Tai, T.C., "Simulation and Analysis of V-22 Rotorcraft Forward-Flight Flowfield", AIAA Paper 95-0046, 33rd Aerospace Sciences Meeting, Reno, Nevada, 1995.

11. Buning, P., et al, "OVERFLOW Users Manual, Version 1.6ah", July 1993.